Scaling relations on high-entropy alloy catalyst surfaces

Ana-Iulia Hutu[a], Emmanouil Pervolarakis[a,b], Ioannis N. Remediakis[b], Henrik H. Kristoffersen*[,a],

Jan Rossmeisl[a]

[a] Department of Chemistry, University of Copenhagen, Copenhagen 2100, Denmark

[b] Department of Materials Science and Technology, University of Crete, Heraklion, 70013, Greece

*E-mail: hhk@chem.ku.dk

Abstract

Scaling and Brønsted-Evans- Polanyi (BEP) relations have proven immensely powerful in catalysis theory. The relations provide an understanding of the Sabatier principle in a quantitative fashion, such that we can calculate the adsorption energy that most optimally compromises between a low reaction barrier and a not too strong adsorption. Scaling and BEP relations are usually mapped out for pure metal surfaces and it is not directly clear how they translate to complex alloy surfaces, e.g. high-entropy alloys (HEAs). The scaling relation between *OH and *OOH is one of the most studied and best understood. Generally, both *OH and *OOH adsorb on a single surface atom, so HEAs do not change the established scaling relation, but rather widen the distribution of available adsorption energies. The situation can be different for reactions at multi-atom surface sites. In the reaction between O* and *CO to form CO_2, the species interact with more surface atoms at the initial state compared to the transition state, so for a given reaction energy, HEAs allow for lower activation energies than pure metals. The reason is that HEA surfaces can make the transition state more similar to the initial state, without the need of steps or other geometric features.

TOC graphic
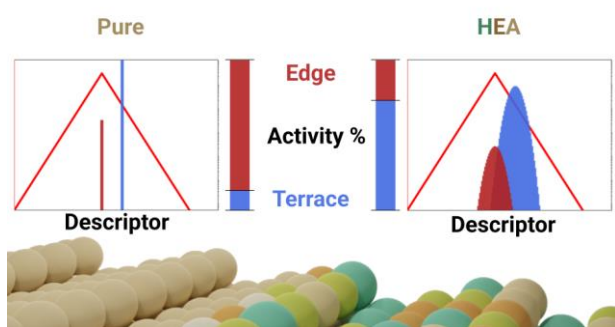
1. Introduction

Scaling and BEP relations have had an immense impact on catalysis theory.[1–4] The observation that adsorption in general is weakened by moving right (from Mn to Cu) and down from 3-d to 5-d among the late transition metals can be rationalized by the d-band model.[5,6] Since any molecule binds weaker going right and down in the periodic table, the binding of the different molecules must all be correlated. It turns out that there often are linear relations between adsorption energies of different molecules, the so-called scaling relations.[7,8] Scaling and BEP relations relate the energies for the states along the reaction path to each other. This means that if you want a low barrier for e.g. dissociation, it requires a stronger adsorption of the atoms, which in turn will be more difficult to react further to the products. This is a formulation of the Sabatier principle, however, the formulation becomes quantitative with scaling and BEP relations. We can calculate what adsorption energy gives the optimal compromise between a low barrier and a not too strong adsorption. A plot of the activity versus adsorption energy is a Sabatier volcano curve.

HEAs (alloys with five or more randomly situated elements) are interesting catalysts, e.g. because one can modify their properties by changing their composition.[63] Furthermore, the heterogeneous HEA surfaces are not governed by mean field behaviors and the removal of mean field approximations in theory development can sometimes provide a deeper understanding of catalysis. One such case concerns scaling and BEP relations, which are usually mapped out on pure metal surfaces. This raises the question of whether these relations are directly applicable to alloy surfaces, especially multi-metallic and HEAs. This is the focus of our paper.

The most shown scaling relation is probably the scaling between *OH and *OOH on metal or oxide surfaces.[9–13] This relation is particular good since both intermediates bind via an oxygen atom and both mostly prefer on top binding on the surface. The *OH and *OOH species are key intermediates in the electrocatalytic oxygen reduction reaction (ORR) and oxygen evolution reaction (OER), which are important reactions for the storage, conversion, and utilization of

renewable electricity. ORR and OER rely heavily on rare materials like Pt and IrO_2. However, alloying the Pt based ORR catalysts with Cu or Ni both cut down on the required amount of Pt and modifies the *OH and *OOH adsorption energies to improve the activity over that of pure Pt. [44, 45] In Section 2, we use ORR and OER to discuss how we expect scaling relations for catalysis at single-atom sites to behave on HEAs. We point out that because both *OH and *OOH adsorb on a single surface atom, HEAs most likely cannot be used to move away from the *OH / *OOH scaling relation. Instead, the *OH and *OOH adsorption energies are continuously distributed on HEAs, rather than having discrete values on pure metal surfaces. This in turn makes geometric features such as step sites less important for ORR and OER on HEAs, since some sites on the flat terraces will adsorb *OH / *OOH with the same strength as step sites.
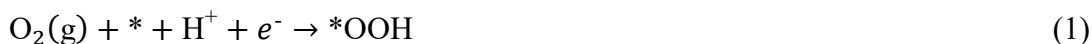
BEP relations[14,15] are a special case of scaling relations, where the linear scaling is observed between the energies of the transition states and the final state of a reaction step, rather than between the adsorption energies of different intermediates. Fast and efficient catalysis is achieved if the energy required to access the transition state is not much higher than the energy of the initial and final states. One way to achieve this is with an "early" (or "late") transition state, where the structure of the transition state is made to resemble the initial state (or final state). Surface defects, such as steps or guest atoms, can often accommodate transition state structures that are more similar to the initial or final states, compared to what is possible on flat defect free terraces.[16–18] In Section 3, we study BEP relations for the CO oxidation reaction, which is a key reaction step in the water-gas shift reaction.[19,20] We specifically consider the reaction between O* and *CO to form CO_2 at multi-atom surface sites and discuss how HEAs can make the transition state more similar to the initial state, without the need of steps or similar geometric defects. An important factor is that the transition state interact with less surface atoms than the initial state, which allows for lower activation energies for a given reaction energy on HEAs than on pure metal surfaces.

4

2. Catalysis at single-atom sites

We first discuss the case where the reaction intermediates primarily adsorb on the same surface atom. In such reactions, the intermediate adsorption energies mostly depend on the element type of the surface atom, but the energies are perturbed by the elements in the local surface environment (ligand effects).[21–24] ORR and OER largely fall into this single-atom site category. We will therefore use ORR (and OER) to highlight how we expect the scaling relations for catalysis at single-atom sites to behave on HEAs.

2.1 The oxygen reduction and evolution reactions.

ORR can evolve through the transfer of either 2 electrons, resulting in hydrogen peroxide, or 4 electrons, resulting in the formation of water. Among the two, the 4-electron path is energetically favored from a thermodynamic point of view and is typically assumed to follow the pathway of eq 1-4,[25–27] also represented in Figure 1a. OER is the reverse pathway, converting H_2O to O_2.

$$O_2(g) + * + H^+ + e^- \rightarrow *OOH \tag{1}$$

$$*OOH + H^+ + e^- \rightarrow O* + H_2O \tag{2}$$

$$O* + H^+ + e^- \rightarrow *OH \tag{3}$$

$$*OH + H^+ + e^- \rightarrow H_2O \tag{4}$$

The four reaction steps have reaction energies given by eq 5-8, where we use the computational hydrogen electrode approach to account for the electric potential.[28]

$$\Delta G_1 = G_{*OOH} - G_* - G_{O_2(g)} - \tfrac{1}{2}G_{H_2(g)} + eU_{vsRHE} = -\Delta G_1^{\{0V\}} + eU_{vsRHE} \tag{5}$$

$$\Delta G_2 = G_{O*} - G_{*OOH} - \tfrac{1}{2}G_{H_2(g)} + eU_{vsRHE} = -\Delta G_2^{\{0V\}} + eU_{vsRHE} \tag{6}$$

$$\Delta G_3 = G_{*OH} - G_{O*} - \tfrac{1}{2}G_{H_2(g)} + eU_{vsRHE} = -\Delta G_3^{\{0V\}} + eU_{vsRHE} \tag{7}$$

$$\Delta G_4 = G_{H_2O(l)} + G_* - G_{*OH} - \tfrac{1}{2}G_{H_2(g)} + eU_{vsRHE} = -\Delta G_4^{\{0V\}} + eU_{vsRHE} \tag{8}$$

5

In eq 5-8, G_* is the free energy of the surface without intermediates, G_{*OOH}, G_{O*}, and G_{*OH} are the free energies of the surface with adsorbates, and $G_{H2O(l)}$, $G_{H2(g)}$, and $G_{O2(g)}$ are the free energies of the molecules. U_{vsRHE} is the electric potential of the electrode/electrocatalyst versus the reversible hydrogen electrode (RHE). Furthermore, we collect the potential independent terms of eq 5-8 into $-\Delta G_1^{\{0V\}}$, $-\Delta G_2^{\{0V\}}$, $-\Delta G_3^{\{0V\}}$, and $-\Delta G_4^{\{0V\}}$, where the minus signs allow us to discuss positive energy differences in the following discussion.

The $O_2(g)$ reduction to two H_2O molecules releases 4.92 eV at 0 V vs RHE (i.e. $\Delta G_1^{\{0V\}} + \Delta G_2^{\{0V\}} + \Delta G_3^{\{0V\}} + \Delta G_4^{\{0V\}} = 4.92$ eV), and ORR/OER therefore have an equilibrium potential of 1.23 V vs RHE. However, ORR can only occur at potentials where all reaction steps are downhill in energy when going from left to right in Figure 1a. The potential where all reaction steps become downhill is called the limiting potential for ORR (U_{ORR}) and is given by eq 9.[25]

$$U_{ORR} = \min(\Delta G_1^{\{0V\}}, \Delta G_2^{\{0V\}}, \Delta G_3^{\{0V\}}, \Delta G_4^{\{0V\}})/e \qquad (9)$$

Similarly, OER can only occur when all steps are downhill going from right to left in Figure 1a. The limiting potential for OER is $U_{OER} = \max(\Delta G_1^{\{0V\}}, \Delta G_2^{\{0V\}}, \Delta G_3^{\{0V\}}, \Delta G_4^{\{0V\}})/e$.

Importantly, ORR/OER catalysts are subject to a stringent scaling relation between the adsorbed *OOH and *OH species, which results in $\Delta G_2^{\{0V\}} + \Delta G_3^{\{0V\}} = 3.2$ eV, with an uncertainty of ±0.2 eV.[9–13] The *OH / *OOH scaling relation is observed to be very universal, which is often explained by the similarities between the *OH and *OOH species. Both intermediates generally adsorb on single surface atoms in on-top positions, have total formal charge of -1e, and can form similar hydrogen bonds. The *OH / *OOH scaling restricts the highest possible limiting potential for ORR to 0.86 V vs RHE, which is obtained when reaction step 1 and 4 share the energy that is not included in the 3.2 eV of the scaling relationship (i.e. $\Delta G_1^{\{0V\}} = \Delta G_4^{\{0V\}} = 0.86$ eV $\leq \Delta G_2^{\{0V\}}$, $\Delta G_3^{\{0V\}}$). The scaling relation simultaneously restricts the optimal OER limiting potential to 1.60 V, which is obtained when $\Delta G_2^{\{0V\}} = \Delta G_3^{\{0V\}} = 1.60$ eV $\geq \Delta G_1^{\{0V\}}$, $\Delta G_4^{\{0V\}}$.

6

The ORR/OER catalysts are also, to a large extend, subject to a scaling relation between *OH and O*, which specify that the energy required to form H_2O from *OH is the same as the energy required to form *OH from O* (i.e. $\Delta G_3^{\{0V\}} = \Delta G_4^{\{0V\}}$). One aspect of this scaling relation is easily rationalized, since if O* is too unstable, it can undergo the following chemical reaction O* + H_2O(l) → 2*OH such that both step 3 and step 4 become conversion of *OH to H_2O(l). This reaction mechanism is sometimes assumed for ORR on Pt(111).[29] The specific energy of the O* species cannot improve the limiting potentials for ORR/OER, when the *OH / *OOH scaling is in effect. However, the O* / *OH scaling does result in catalysts not being bidirectional for ORR and OER (i.e. catalysts do not catalyze ORR and OER equally well). The optimal ORR catalyst subject to both *OH / *OOH scaling and O* / *OH scaling has $\Delta G_1^{\{0V\}} = \Delta G_4^{\{0V\}} = \Delta G_3^{\{0V\}} = 0.86$ eV, and $\Delta G_2^{\{0V\}} = 2.34$ eV, while the optimal OER catalyst has $\Delta G_2^{\{0V\}} = \Delta G_3^{\{0V\}} = \Delta G_4^{\{0V\}} = 1.60$ eV, and $\Delta G_1^{\{0V\}} = 0.12$ eV (Figure 1b). The optimal catalyst subject to *OH / *OOH scaling, but not O* / *OH scaling has $\Delta G_1^{\{0V\}} = \Delta G_4^{\{0V\}} = 0.86$ eV and $\Delta G_2^{\{0V\}} = \Delta G_3^{\{0V\}} = 1.60$ eV, and is bidirectional, with 0.37 V overpotential for both ORR and OER. Interestingly, catalysts with bidirectional properties and overpotentials around 0.37 have been reported in the literature.[30] This shows that O* / *OH scaling can be broken.
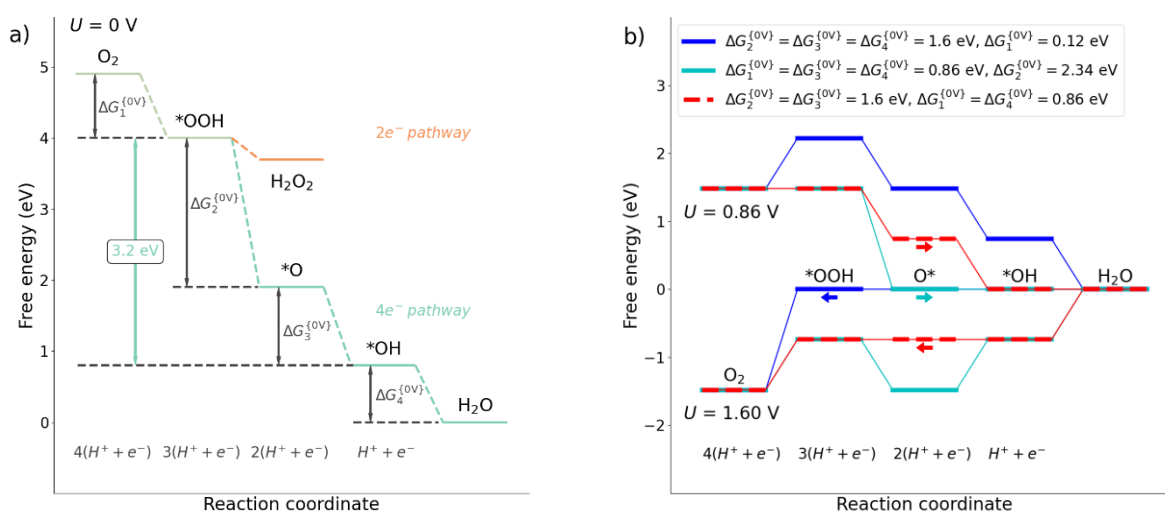
Figure 1: (a) Free energy diagram for the ORR at $U = 0$ V vs RHE. (b) Free energy diagrams at $U = 0.86$ and $U = 1.60$ V vs RHE. The optimal ORR catalyst subject to O*/*OH scaling is plotted in cyan, the optimal OER catalyst subject to O*/*OH scaling is plotted in blue, and the optimal bidirectional catalyst not subject to O*/*OH scaling is plotted in red. The arrows show pathways that are active in the indicated directions.

The *OH / *OOH scaling relationship has been observed on both HEAs[31] and at steps and other undercoordinated sites on pure metal surfaces.[32] This emphasizes the universality of the $\Delta G_2^{\{0V\}} + \Delta G_3^{\{0V\}} = 3.2$ eV ± 0.2 eV scaling relation, and the challenge of lowering the overpotential below 0.37 V for both ORR and OER.[26,27] Oppositely, the O* / *OH scaling relation is easily broken on HEAs, simply because *OH usually adsorb in on-top positions, while O* adsorb in threefold hollow sites and therefore interact directly with three surface atoms instead of one.[31]

If we accept that the *OH / *OOH scaling relation cannot be subverted, then the search for the most active ORR catalyst becomes a search for surfaces with optimum *OH adsorption energy (i.e. $\Delta G_4^{\{0V\}} = 0.86$ eV). ORR catalysts with optimum *OH adsorption energy could still have low activity, if the O* formation step ($\Delta G_3^{\{0V\}}$) is prohibitive, however, that step has to fall outside the [0.86 eV, 2.34 eV] energy window in order to restrict the ORR activity.

Pt is one of the best performing ORR electrocatalysts,[33,34] even though the Pt(111) surface adsorbs *OH 0.1 eV too strongly.[35] One strategy is, therefore, to modify Pt(111) just enough that it adsorbs *OH 0.1 eV weaker. Pt facets with less coordinated atoms than (111) doesn't improve the ORR activity, since these surfaces typically are more reactive than Pt(111) and adsorb *OH stronger instead of weaker.[36,37] However, Pt surfaces with short (111) terraces separated by monatomic steps do have increased ORR activity, compared to completely flat Pt(111) surfaces.[38–41] The reason may be that *OH is less solvated by the aqueous electrolyte on short terraces.[42] Another successful

strategy is to alloy Pt with elements that weaken the *OH adsorption energy,[43] examples are Pt$_3$Ni [44] and Pt with Cu in subsurface layers.[45] This strategies work by placing more reactive metal atoms in the vicinity of the Pt(111) atoms that adsorb *OH. These adjacent atoms interact strongly with Pt(111), which in turn weakens the interaction between Pt(111) and *OH.[46,47]

In Figure 2, we have illustrated the *OH / *OOH scaling relationship as a line with slope 1 and y-axis intercept at 3.2 eV. As discussed for Pt, one can use structure effects to move up and down the line. However, changing the surface structure will move the *OH adsorption free energy a finite amount on the scaling line, so the adjustability is limited. For instance, *OH adsorption free energies are stabilized by around 0.25 eV at (553) step sites compared to (111) terrace sites, largely independent of the metal in question.[32] HEAs can also be used to move up and down on the line, but instead of the finite shift expected when changing the surface structure, the heterogeneous nature of HEA surfaces convert the distinct *OH / *OOH adsorption energies into a continuum of adsorption energies (ensemble effect).[48–50] Specifically, each element adsorb *OH close to the value of the pure metal, but with Gaussian distributed adsorption energies due to the perturbation from the other elements in the surface. E.g., on the equimolar IrPdPtRhRu (111) surface, each element covers an *OH adsorption energy range of almost 0.5 eV and the five elements combined covers nearly 1.5 eV. [48] This means that a fraction of the HEA surface sites will have the optimum *OH adsorption energy.
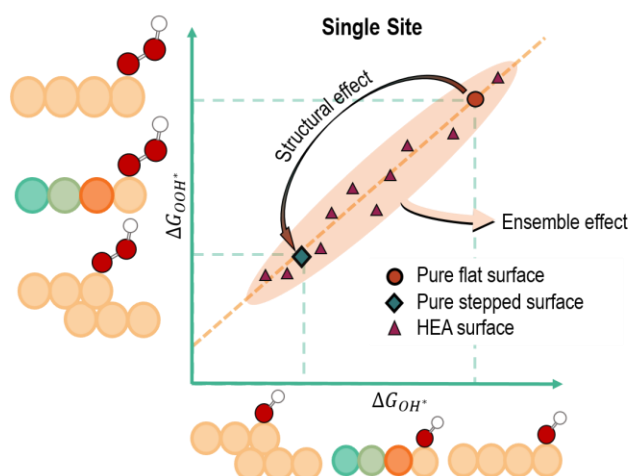
Figure 2: Scaling relation between the energies of *OOH and *OH intermediates in the case of ORR, for flat and stepped pure metal surfaces, as well as HEA surfaces.

It might be possible to get an active catalyst by having a small portion of the *OH / *OOH adsorption sites at the optimal adsorption energy. This is reminiscent of cases where structural defects in extended surfaces or edges and vertices of nanoparticles account for most of the catalytic activity, even though they make up a small fraction of the surface sites.[51–54] We have already mentioned that geometric features, like steps or narrow Pt(111) terraces, are a common way to expand the available adsorption energies of a material. In general, more undercoordinated sites result in stronger adsorption. However, undercoordinated geometric features are also unstable and consequently scarcer than higher coordinated surface atoms. Alloys, on the other hand, especially HEAs, provide a wide adsorption energy distribution[48] without the same scarcity issue. Figure 3 illustrates *OH adsorption energy distributions on a hypothetical pure metal with surface defects (e.g. monoatomic steps) (Figure 3a) and on a hypothetical HEA (Figure 3b). We further overlay the ORR limiting potential and estimate the catalytic activity with an Arrhenius-like expression, using the surface site fraction, a temperature of 300K, pre-exponential factor of 1, and a potential of 0.86 V vs RHE. This is similar to the estimated kinetic limited current in [[55]]. In the pure metal case, we

10

assume the flat surfaces have *OH adsorption at $\Delta G_4^{\{0V\}} = 1.06$ eV and monoatomic steps have *OH adsorption at $\Delta G_4^{\{0V\}} = 0.86$ eV, and assign them the fractions $1 : 3 \cdot 10^{-3}$. With these assumptions, the monoatomic steps (Figure 3a, left bar) account for most of the activity (87%), even though they are several orders of magnitude less in number compared to the flat surfaces (right bar).

The rich configurational space of HEA surfaces create continuous *OH adsorption site distributions shaped as Gaussians.[48–50] In our hypothetical HEA case, we therefore convert the pure metal single valued *OH adsorption sites into Gaussian distributions with the same number of sites, centered at the same *OH adsorption energies, but with standard deviations of 0.05 eV (Figure 3b). The effect is that less of the monoatomic steps are at the optimal *OH adsorption energy, and the step sites only account for 27% of the total activity. Oppositely, the terrace sites account for 73% of the total activity, because fractions of the terrace sites are at or close to the optimal value. The two hypothetical cases have roughly the same total activity ($3.4 \cdot 10^{-3}$ s^{-1} per pure element site and $3.8 \cdot 10^{-3}$ s^{-1} per HEA site). We note that the relative importance of step sites verses terrace sites depend a lot on the standard deviation for the Gaussian *OH adsorption energy distributions. The 0.05 eV that we have chosen, is similar to values reported in the literature [64] , but larger values will make step sites less important.
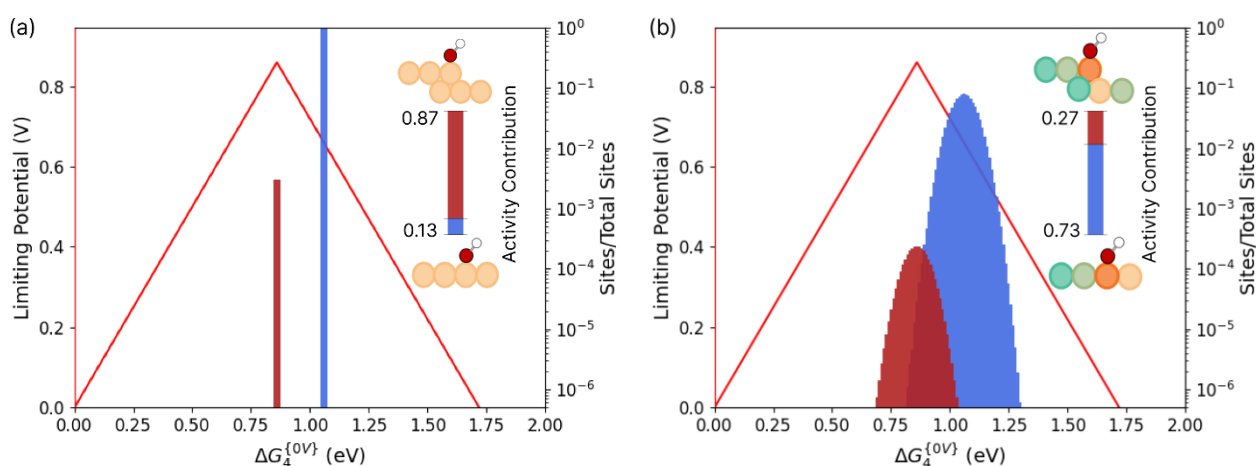
Figure 3: (a) *OH adsorption energy distributions for a hypothetical pure metal with terrace sites

($\Delta G_4^{\{0V\}}$ = 1.06 eV) and step sites ($\Delta G_4^{\{0V\}}$ = 0.86 eV). (b) *OH adsorption energy distributions for a hypothetical HEA surface with Gaussian distributed terrace sites (centered at $\Delta G_4^{\{0V\}}$ = 1.06 eV and with 0.05 eV standard deviation) and step sites (centered at $\Delta G_4^{\{0V\}}$ = 0.86 eV and with 0.05 eV standard deviation). The fraction of terrace versus step sites is $1 : 3 \cdot 10^{-3}$. The figures also contain a plot of the limiting potential volcano. The right y-axis represents the number of sites and the color bar shows the partial contribution from terraces and steps to the total activity. The activity is calculated with an Arrhenius-like expression, [55] using the surface site fraction, a temperature of 300K, pre-exponential factor of 1, and a potential of 0.86 V vs RHE.

3. Catalysis at multi-atom sites

The element makeup of HEA surfaces could be more crucial for reactions that involve more than one surface atom, especially if the intermediates and transition states interact with a varying number of surface atoms. To illustrate this, we use the CO oxidation reaction (COOR) as an example.

3.1 The CO oxidation reaction.

The COOR between adsorbed *CO and O* (eq 10) on multi-metallic (111) surfaces was studied in [[56]].

$$O* + *CO \rightarrow CO_2(g) \tag{10}$$

The study assumed that eq 10 is the key reaction step in the water gas shift reaction (i.e. $CO(g) + H_2O(g) \rightarrow CO_2(g) + H_2(g)$). Figure 4a illustrates the DFT energy landscape for the water gas shift reaction modeled on Pt(111). The O* species is formed by H_2O dissociation and generally prefers to adsorb at a threefold hollow site, whereas *CO adsorb directly from the gas phase and generally prefers to sit at an on-top position. We, therefore, (at a minimum) need to keep track of three surface atoms (*A, B, C*) to capture O* adsorption, and one adjacent surface atom (*D*) to capture *CO

12

adsorption. Figure 4b illustrate the COOR active site made up of these four surface atoms. Ligand effects further complicate the picture, but we will ignore these in this section.
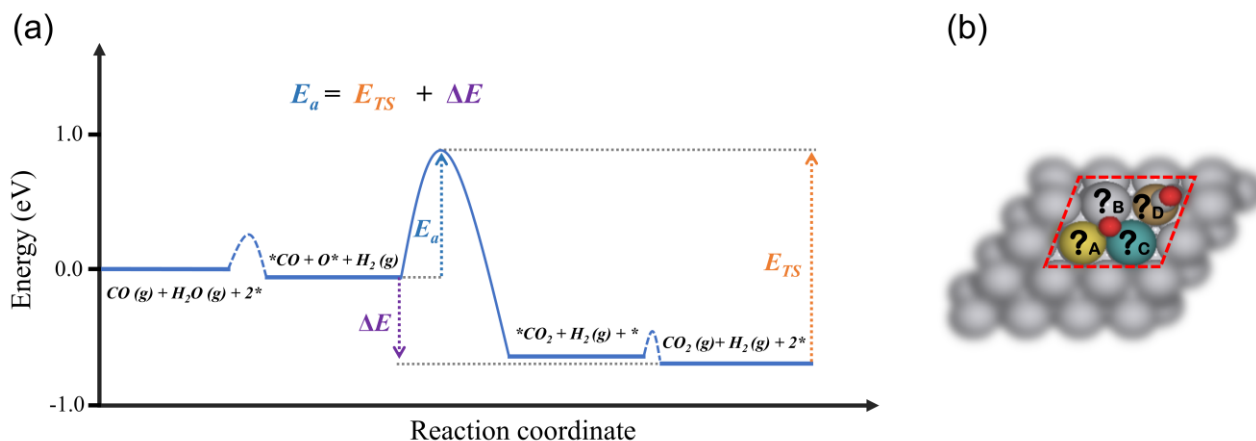
Figure 4: (a) DFT energy diagram for the water-gas shift reaction on the Pt(111) surface. E_{TS} is the energy of the transition state compared to the energy of the products (CO_2(g) and H_2(g)). E_a is the activation energy and ΔE is the reaction energy of the *CO + O* → CO_2(g) reaction step. (b) Illustration of the four adjacent metal atoms directly involved in COOR. The O* atom binds to atoms *A, B* and *C*, while *CO adsorbs at atom *D*. Reprinted with permission from ref.[56] Copyright 2022 American Chemical Society.

The DFT reaction energy (ΔE) of eq 10 is given by eq 11. We add the "(A,B,C,D)" superscript to indicate that ΔE depends on the element makeup of the active site.

$$\Delta E^{(A,B,C,D)} = -0.73\text{eV} - \left(E_{O*}^{(A,B,C)} + E_{*CO}^{(D)} \right) \tag{11}$$

The -0.73 eV is the DFT reaction energy of the full water gas shift reaction, $E_{O*}^{(A,B,C)}$ is the adsorption energy of O* (formed from H_2O(g)) at the *A, B, C* surface site, and $E_{*CO}^{(D)}$ is the adsorption energy of *CO on atom *D*. The activation energy (E_a) of eq 10 also depends on the (A,B,C,D) element makeup of the active site. However, at the COOR transition state, the O* species

13

have moved away from the threefold hollow site to a bridge position between the *B, C* surface atoms, while *CO remains at the *D* surface atom. This means that the activation energy of the backwards eq 10 reaction ($E_{TS}^{(B,C,D)}$) does not depend on surface atom *A* and is therefore a more convenient transition state descriptor than $E_a^{(A,B,C,D)}$. The $\Delta E^{(A,B,C,D)}$, $E_a^{(A,B,C,D)}$ and $E_{TS}^{(B,C,D)}$ are related by eq 12.

$$E_a^{(A,B,C,D)} = E_{TS}^{(B,C,D)} + \Delta E^{(A,B,C,D)} \tag{12}$$

Studies of COOR have found that E_a scales linearly with ΔE on pure metals.[57,58] However, HEAs may not be subject to the same limitations.[59] We could investigate to what extend HEAs are subject to scaling based restrictions between ΔE and E_a by calculating COOR on multiple HEA surface sites in a brute force approach. However, a less accurate, but perhaps more insightful, approach is to approximate how $E_{*CO}^{(D)}$, $E_{O*}^{(A,B,C)}$, and $E_{TS}^{(B,C,D)}$ depend on the makeup of the *A, B, C, D* active site. The study,[56] therefore, proceeded to estimate $E_{O*}^{(A,B,C)}$ and $E_{TS}^{(B,C,D)}$ as being linearly dependent on on-top O* and *CO adsorption energies ($E_{*CO}^{(D)}$ is used as an input, since it's an on-top adsorption energy that mainly depends on atom *D*). The $E_{O*}^{(A,B,C)}$ values were approximated by eq 13, where $E_{O*,top}^{(A)}$, $E_{O*,top}^{(B)}$, $E_{O*,top}^{(C)}$ are O* on-top adsorption energies on the three atoms making up the hollow site. The -1.26 eV is added, because hollow sites are significantly more stable than on-top adsorption sites.

$$E_{O*}^{(A,B,C)} \simeq \frac{1}{3}\left(E_{O*,top}^{(A)} + E_{O*,top}^{(B)} + E_{O*,top}^{(C)}\right) - 1.26\text{eV} \tag{13}$$

Similarly, $E_{TS}^{(B,C,D)}$ was approximated by eq 14, which depends on $E_{O*,top}^{(B)}$, $E_{O*,top}^{(C)}$, and $E_{*CO}^{(D)}$, because the transition state has O* adsorbed at a *B, C* bridge position and *CO adsorbed on atom *D*.

$$E_{TS}^{(B,C,D)} \simeq 0.61 \cdot \left(E_{*CO}^{(D)} + \frac{1}{2}\left(E_{O*,top}^{(B)} + E_{O*,top}^{(C)}\right)\right) + 1.01\text{eV} \tag{14}$$

Reference [56] provides additional details regarding the fitting of eq 13 and eq 14 to computed adsorption and transition state energies.

The approximations for $E_{O*}^{(A,B,C)}$ and $E_{TS}^{(B,C,D)}$ allow us to explore what ΔE (eq 11) and E_a (eq 12) values are possible. $E_{O*,top}^{(A)}$ ranges from 0.88 eV on Ru(111) to 3.88 eV on Au(111), whereas E_{*CO} ranges from -1.70 eV on Ru(111) to around 0 eV on Au(111) and Ag(111). On pure metal (111) surfaces, the three O* on-top adsorption energies are equal (i.e. $E_{O*,top}^{(A)} = E_{O*,top}^{(B)} = E_{O*,top}^{(C)}$), and, in that case, E_a falls on a single line (black line in Figure 5), no matter what values of $E_{O*,top}^{(A)}$ we pick in the ranges between Ru(111) and Au(111). Note that since $E_{*CO}^{(D)}$ and the combined O* adsorption energy have the same weight in both $E_{O*}^{(A,B,C)}$ and $E_{TS}^{(B,C,D)}$, changing $E_{*CO}^{(D)}$ still gives E_a values on the black line. Figure 5 includes DFT calculated ΔE and E_a for pure metals (red circles) from ref [56], which show that the black scaling line is a decent representation of pure metals, even though the approximations were made to describe multi-metallic surfaces. The standard deviation between the predicted and calculated E_a and ΔE values for pure metals are 0.21 eV and 0.24 eV, respectively.

The possible values of ΔE and E_a are much less restricted on HEAs, which we emulate with adsorption energies in the range between adsorption on Au(111) and on Ru(111), but with $E_{O*,top}^{(A)} \neq E_{O*,top}^{(B)} \neq E_{O*,top}^{(C)}$ (gray area in Figure 5). The reason for the lessening of restrictions is that O* interacts with three atoms (*A, B, C*) at the initial state, but only two atoms (*B, C*) at the transition state. The blue squares in Figure 5 are DFT calculated ΔE and E_a values on multi-metallic surfaces from ref [56], and they confirm that the possible values of ΔE and E_a have expanded. Many of the calculated squares are close to the outer boundary of the gray area, and could be the optimal COOR active sites achievable on HEAs. Still, the optimal sites on HEA surfaces are far from ideal COOR catalytic sites (the gray area is not close to the "Ideal" yellow lines), which would be achieved if the reaction had no barrier (i.e. $E_a = 0$), or no additional barrier beyond an uphill reaction energy (i.e. $E_a = \Delta E$).

Finally, we would like to mention two additional considerations about the ΔE and E_a relations in Figure 5. First, the gray area is very similar in shape to the achievable catalytic sites for N_2

dissociation on AuCoFeMoRu, mapped out with a brute force approach.[60] This indicate that the analysis we have done for COOR is more general, and highlights the potential of adding additional elements to a catalyst. Secondly, HEAs can lower the activation energy of COOR without the need for geometric defects, which is otherwise the main way to improve the catalytic activity of pure metals.[61,62] This observation is important for HEA catalysis research, as it shows that geometric effects are less crucial on HEAs, so perhaps geometric effects should receive less focus than other aspects of HEA catalysis.
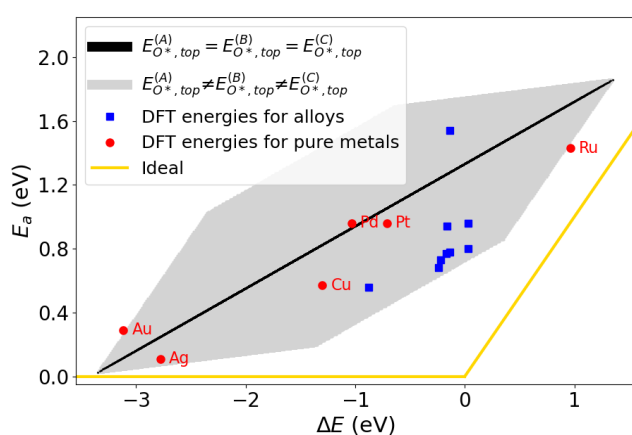
Figure 5: Relation between ΔE and E_a estimated by eq 13 and eq 14, respectively, with $E_{O^*,top}^{(A)}$, $E_{O^*,top}^{(B)}$, $E_{O^*,top}^{(C)} \in \{0.88 \text{ eV}, 3.88 \text{ eV}\}$, and $E_{*CO}^{(D)} \in \{-1.70 \text{ eV}, 0 \text{ eV}\}$. We have also plotted ΔE and E_a from DFT calculations on pure metals (red circles) and alloy (111) surfaces (blue squares), and the ideal situation, i.e. $E_a = \max(0, \Delta E)$ (yellow lines). The DFT calculations are from [[56]].

4. Summary

We have discussed how scaling and BEP relations apply to HEA surface catalysis. In the case of ORR and OER, literature data indicate that HEAs do not alter the important and restrictive scaling relation between *OH and *OOH, mainly because both intermediates interact with a single surface metal atom. The role of HEAs is rather to broaden the distribution of *OH and *OOH adsorption energies.

16

This reduces the relevance of geometric defects, which are often relied on to modify adsorption energies. In CO oxidation, HEAs can make the transition state more similar to the initial state, because the transition state interacts with less surface atoms than the initial state. This allows for lower activation energies for a given reaction energy on HEAs than on pure metal surfaces. The ability to get transition states that are more similar to the initial or final states is again usually associated with surface defects. We, therefore, surmise that HEAs affect scaling and BEP relations in ways similar to geometric defects, and are, therefore, less reliant on the presence of geometric defects. Finally, an important aspect of scaling and BEP relations are the limitations they put on the performance of most catalytic reactions. These restrictions often make ideal catalysis (catalysis without reaction barriers) unachievable. It is worth noticing that even the high flexibility of HEAs does not allow for ideal ORR, OER, or COOR catalysts. This further solidifies that it is likely fundamentally impossible to design ideal catalysts for these reactions.

Author biographies

Ana-Iulia Hutu

Ana-Iulia Hutu is a PhD student at the Center for High-Entropy Alloy Catalysis (CHEAC), Department of Chemistry, University of Copenhagen, Denmark, under the supervision of Jan Rossmeisl. She earned her BSc and MSc in Chemistry from 'Alexandru Ioan Cuza' University in Iasi, Romania. Her research centers on modeling catalytic reactions of small molecules using density functional theory calculations and micro-kinetic modeling, with a specific interest in the nitrogen reduction reaction.

Emmanouil Pervolarakis

Emmanouil Pervolarakis holds a BSc in Physics, an MSc and a PhD in Materials Science and Technology, all awarded from the University of Crete. Currently, he is a postdoctoral researcher at the Center for High-Entropy Alloy Catalysis, Department of Chemistry, University of Copenhagen. His research focuses on accelerating materials discovery, particularly for high entropy alloys, through the application of data science and machine learning techniques.

Ioannis N. Remediakis

Ioannis Remediakis is Associate Professor at the Department of Materials Science and Engineering, University of Crete, Greece, and affiliated research Scientist at the Foundation for Research and Technology - Hellas (FORTH). He got his bachelor (1997), masters (1998), PhD (2002) degrees from the University of Crete. Before returning to Crete as faculty, he had worked at Harvard University, USA, the University of Ioannina, Greece and the Technical University of Denmark. His research involves first-principles computer simulations for low-dimensional systems with applications to

nano-chemistry (shape and properties of metal nanoparticles, heterogeneous catalysis) and nano-physics (two-dimensional semiconductors, nanostructured solids).

Henrik H. Kristoffersen

Henrik Kristoffersen is postdoctoral researcher at the Center for High-Entropy Alloy Catalysis, Department of Chemistry, University of Copenhagen. He got his Ph.D. (2013) in Nanoscience at Aarhus University, Denmark, and has later worked at UC Santa Barbara, USA, and Technical University of Denmark. His research interests include; modeling of electrochemistry, liquid-solid interfaces, reducible oxides, and heterogeneous catalysis.

Jan Rossmeisl

Jan Rossmeisl is Professor of theoretical chemistry and he heads the Center for High Entropy Alloy Catalysis at the Department of Chemistry at Copenhagen University. Before joining the University of Copenhagen in April 2015, he was an Associate Professor and group leader for the theoretical catalysis group at the Department of Physics at the Technical University of Denmark. He holds master's (2000) and Ph.D. (2004) degrees in physics from the Technical University of Denmark. His research interests include electrocatalysis, energy conversion, atomic scale simulations, and rational interface design for catalysis.

References

(1)   Bligaard, T.; Nørskov, J. K.; Dahl, S.; Matthiesen, J.; Christensen, C. H.; Sehested, J. The Brønsted–Evans–Polanyi Relation and the Volcano Curve in Heterogeneous Catalysis. *J. Catal.* **2004**, *224*, 206–217.

(2)   van Santen, R. A.; Neurock, M.; Shetty, S. G. Reactivity Theory of Transition-Metal Surfaces: A Brønsted−Evans−Polanyi Linear Activation Energy−Free-Energy Analysis. *Chem. Rev.* **2010**, *110*, 2005–2048.

(3)   Greeley, J. Theoretical Heterogeneous Catalysis: Scaling Relationships and Computational Catalyst Design. *Annu. Rev. Chem. Biomol. Eng.* **2016**, *7*, 605–635.

(4)   Metiu, H.; Agarwal, V.; Kristoffersen, H. H. THE ROLE OF COMPUTATIONS IN CATALYSIS. In *Reviews in Computational Chemistry*; Parrill, A. L., Lipkowitz, K. B., Eds.; Wiley, 2018; Vol. 31, p 171.

(5)   Hammer, B.; Nørskov, J. K. Why Gold Is the Noblest of All the Metals. *Nature* **1995**, *376*, 238–240..

(6)   Hammer, B.; Nørskov, J. K. Electronic Factors Determining the Reactivity of Metal Surfaces. *Surf. Sci.* **1995**, *343*, 211–220.

(7)   Nørskov, J. K.; Bligaard, T.; Logadottir, A.; Bahn, S.; Hansen, L. B.; Bollinger, M.; Bengaard, H.; Hammer, B.; Sljivancanin, Z.; Mavrikakis, M.; Xu, Y.; Dahl, S.; Jacobsen, C. J. H. Universality in Heterogeneous Catalysis. *J. Catal.* **2002**, *209*, 275–278.

(8)   Medford, A. J.; Vojvodic, A.; Hummelshøj, J. S.; Voss, J.; Abild-Pedersen, F.; Studt, F.; Bligaard, T.; Nilsson, A.; Nørskov, J. K. From the Sabatier Principle to a Predictive Theory of Transition-Metal Heterogeneous Catalysis. *J. Catal.* **2015**, *328*, 36–42.

(9)   Rossmeisl, J.; Logadottir, A.; Nørskov, J. K. Electrolysis of Water on (Oxidized) Metal Surfaces. *Chem. Phys.* **2005**, *319*, 178–184.

(10)   Koper, M. T. M. Thermodynamic Theory of Multi-Electron Transfer Reactions: Implications for Electrocatalysis. *J. Electroanal. Chem.* **2011**, *660*, 254–260.

(11)   Man, I. C.; Su, H.-Y.; Calle-Vallejo, F.; Hansen, H. A.; Martínez, J. I.; Inoglu, N. G.; Kitchin, J.; Jaramillo, T. F.; Nørskov, J. K.; Rossmeisl, J. Universality in Oxygen Evolution Electrocatalysis on Oxide Surfaces. *ChemCatChem* **2011**, *3*, 1159–1165.

(12)   Calle-Vallejo, F.; Martínez, J. I.; Rossmeisl, J. Density Functional Studies of Functionalized Graphitic Materials with Late Transition Metals for Oxygen Reduction Reactions. *Phys. Chem. Chem. Phys.* **2011**, *13*, 15639–15643.

(13)   Viswanathan, V.; Hansen, H. A.; Rossmeisl, J.; Nørskov, J. K. Universality in Oxygen Reduction Electrocatalysis on Metal Surfaces. *ACS Catal.* **2012**, *2*, 1654–1660.

(14)   Bronsted, J. N. Acid and Basic Catalysis. *Chem. Rev.* **1928**, *5*, 231–338.

(15)   Evans, M. G.; Polanyi, M. Inertia and Driving Force of Chemical Reactions. *Trans. Faraday Soc.* **1938**, *34*, 11–24.

(16)   Nørskov, J. K.; Bligaard, T.; Hvolbæk, B.; Abild-Pedersen, F.; Chorkendorff, I.; Christensen, C. H. The Nature of the Active Site in Heterogeneous Metal Catalysis. *Chem. Soc. Rev.* **2008**, *37*, 2163–2171.

(17)   Koper, M. T. M. Structure Sensitivity and Nanoscale Effects in Electrocatalysis. *Nanoscale* **2011**, *3*, 2054–2073.

(18) Darby, M. T.; Réocreux, R.; Sykes, E. Charles. H.; Michaelides, A.; Stamatakis, M. Elucidating the Stability and Reactivity of Surface Intermediates on Single-Atom Alloy Catalysts. *ACS Catal.* **2018**, *8*, 5038–5050.

(19) Ratnasamy, C.; Wagner, J. P. Water Gas Shift Catalysis. *Chem. Rev.* **2009**, *51*, 325–440.

(20) Baraj, E.; Ciahotný, K.; Hlinčík, T. The Water Gas Shift Reaction: Catalysts and Reaction Mechanism. *Fuel* **2021**, *288*, 119817.

(21) Clausen, C. M.; Batchelor, T. A. A.; Pedersen, J. K.; Rossmeisl, J. What Atomic Positions Determines Reactivity of a Surface? Long-Range, Directional Ligand Effects in Metallic Alloys. *Adv. Sci.* **2021**, *8*, 2003357.

(22) Asano, M.; Kawamura, R.; Sasakawa, R.; Todoroki, N.; Wadayama, T. Oxygen Reduction Reaction Activity for Strain-Controlled Pt-Based Model Alloy Catalysts: Surface Strains and Direct Electronic Effects Induced by Alloying Elements. *ACS Catal.* **2016**, *6*, 5285–5289.

(23) Schlapka, A.; Lischka, M.; Groß, A.; Käsberger, U.; Jakob, P. Surface Strain versus Substrate Interaction in Heteroepitaxial Metal Layers: Pt on Ru(0001). *Phys. Rev. Lett.* **2003**, *91*, 16101.

(24) Hoster, H. E.; Alves, O. B.; Koper, M. T. M. Tuning Adsorption via Strain and Vertical Ligand Effects. *ChemPhysChem* **2010**, *11*, 1518–1524.

(25) Busch, M.; Halck, N. B.; Kramm, U. I.; Siahrostami, S.; Krtil, P.; Rossmeisl, J. Beyond the Top of the Volcano? – A Unified Approach to Electrocatalytic Oxygen Reduction and Oxygen Evolution. *Nano Energy* **2016**, *29*, 126–135.

(26) Seh, Z. W.; Kibsgaard, J.; Dickens, C. F.; Chorkendorff, I.; Nørskov, J. K.; Jaramillo, T. F. Combining Theory and Experiment in Electrocatalysis: Insights into Materials Design. *Science* **2017**, *355*, eaad4998.

(27) Chen, W.; Huang, J.; Wei, J.; Zhou, D.; Cai, J.; He, Z.-D.; Chen, Y.-X. Origins of High Onset Overpotential of Oxygen Reduction Reaction at Pt-Based Electrocatalysts: A Mini Review. *Electrochem. Commun.* **2018**, *96*, 71–76.

(28) Nørskov, J. K.; Rossmeisl, J.; Logadottir, A.; Lindqvist, L.; Kitchin, J. R.; Bligaard, T.; Jónsson, H. Origin of the Overpotential for Oxygen Reduction at a Fuel-Cell Cathode. *J. Phys. Chem. B* **2004**, *108*, 17886–17892.

(29) Tripković, V.; Skúlason, E.; Siahrostami, S.; Nørskov, J. K.; Rossmeisl, J. The Oxygen Reduction Reaction Mechanism on Pt(111) from Density Functional Theory Calculations. *Electrochim. Acta* **2010**, *55*, 7975–7981.

(30) Morales, D. M.; Kazakova, M. A.; Dieckhöfer, S.; Selyutin, A. G.; Golubtsov, G. V; Schuhmann, W.; Masa, J. Trimetallic Mn-Fe-Ni Oxide Nanoparticles Supported on Multi-Walled Carbon Nanotubes as High-Performance Bifunctional ORR/OER Electrocatalyst in Alkaline Media. *Adv. Funct. Mater.* **2020**, *30*, 1905992.

(31) Pedersen, J. K.; Batchelor, T. A. A.; Yan, D.; Skjegstad, L. E. J.; Rossmeisl, J. Surface Electrocatalysis on High-Entropy Alloys. *Curr. Opin. Electrochem.* **2021**, *26*, 100651.

(32) Calle-Vallejo, F.; Loffreda, D.; Koper, M. T. M.; Sautet, P. Introducing Structural Sensitivity into Adsorption–Energy Scaling Relations by Means of Coordination Numbers. *Nat. Chem.* **2015**, *7*, 403–410.

(33) Nie, Y.; Li, L.; Wei, Z. Recent Advancements in Pt and Pt-Free Catalysts for Oxygen Reduction Reaction. *Chem. Soc. Rev.* **2015**, *44*, 2168–2201.

(34) Xia, W.; Mahmood, A.; Liang, Z.; Zou, R.; Guo, S. Earth-Abundant Nanomaterials for Oxygen Reduction. *Angew. Chem. Int. Ed.* **2016**, *55*, 2650–2676.

(35) Garcia-Araez, N. Standard Adsorption Gibbs Energy for Hydrogen, OH, Chloride, and Sulfate on Pt(111): Comparison of Different Isotherms. *J. Phys. Chem. C* **2011**, *115*, 3075–3082.

(36) Rizo, R.; Herrero, E.; Feliu, J. M. Oxygen Reduction Reaction on Stepped Platinum Surfaces in Alkaline Media. *Phys. Chem. Chem. Phys.* **2013**, *15*, 15416–15425.

(37) Perez-Alonso, F. J.; McCarthy, D. N.; Nierhoff, A.; Hernandez-Fernandez, P.; Strebel, C.; Stephens, I. E. L.; Nielsen, J. H.; Chorkendorff, I. The Effect of Size on the Oxygen Electroreduction Activity of Mass-Selected Platinum Nanoparticles. *Angew. Chem. Int. Ed.* **2012**, *51*, 4641–4643.

(38) Bandarenka, A. S.; Hansen, H. A.; Rossmeisl, J.; Stephens, I. E. L. Elucidating the Activity of Stepped Pt Single Crystals for Oxygen Reduction. *Phys. Chem. Chem. Phys.* **2014**, *16*, 13625–13629.

(39) Kuzume, A.; Herrero, E.; Feliu, J. M. Oxygen Reduction on Stepped Platinum Surfaces in Acidic Media. *J. Electroanal. Chem.* **2007**, *599*, 333–343.

(40) Hitotsuyanagi, A.; Nakamura, M.; Hoshi, N. Structural Effects on the Activity for the Oxygen Reduction Reaction on n(111)–(100) Series of Pt: Correlation with the Oxide Film Formation. *Electrochim. Acta* **2012**, *82*, 512–516.

(41) Kodama, K.; Jinnouchi, R.; Takahashi, N.; Murata, H.; Morimoto, Y. Activities and Stabilities of Au-Modified Stepped-Pt Single-Crystal Electrodes as Model Cathode Catalysts in Polymer Electrolyte Fuel Cells. *J. Am. Chem. Soc.* **2016**, *138*, 4194–4200.

(42) Nagoya, A.; Jinnouchi, R.; Kodama, K.; Morimoto, Y. DFT Calculations on H, OH and O Adsorbate Formations on Pt(322) Electrode. *J. Electroanal. Chem.* **2015**, *757*, 116–127.

(43) Stephens, I. E. L.; Bondarenko, A. S.; Grønbjerg, U.; Rossmeisl, J.; Chorkendorff, I. Understanding the Electrocatalysis of Oxygen Reduction on Platinum and Its Alloys. *Energy Environ. Sci.* **2012**, *5*, 6744–6762.

(44) Stamenkovic, V. R.; Fowler, B.; Mun, B. S.; Wang, G.; Ross, P. N.; Lucas, C. A.; Marković, N. M. Improved Oxygen Reduction Activity on Pt3Ni(111) via Increased Surface Site Availability. *Science* **2007**, *315*, 493–497.

(45) Jensen, K. D.; Tymoczko, J.; Rossmeisl, J.; Bandarenka, A. S.; Chorkendorff, I.; Escudero-Escribano, M.; Stephens, I. E. L. Elucidation of the Oxygen Reduction Volcano in Alkaline Media Using a Copper–Platinum(111) Alloy. *Angew. Chem. Int. Ed.* **2018**, *57*, 2800–2805.

(46) Knudsen, J.; Nilekar, A. U.; Vang, R. T.; Schnadt, J.; Kunkes, E. L.; Dumesic, J. A.; Mavrikakis, M.; Besenbacher, F. A Cu/Pt Near-Surface Alloy for Water−Gas Shift Catalysis. *J. Am. Chem. Soc.* **2007**, *129*, 6485–6490.

(47) Matanović, I.; Garzon, F. H.; Henson, N. J. Theoretical Study of Electrochemical Processes on Pt–Ni Alloys. *J. Phys. Chem. C* **2011**, *115*, 10640–10650.

(48) Batchelor, T. A. A.; Pedersen, J. K.; Winther, S. H.; Castelli, I. E.; Jacobsen, K. W.; Rossmeisl, J. High-Entropy Alloys as a Discovery Platform for Electrocatalysis. *Joule* **2019**, *3*, 834–845.

(49) Pedersen, J. K.; Batchelor, T. A. A.; Bagger, A.; Rossmeisl, J. High-Entropy Alloys as Catalysts for the CO_2 and CO Reduction Reactions. *ACS Catal.* **2020**, *10*, 2169–2176.

(50) Yan, D.; Kristoffersen, H. H.; Castelli, I. E.; Rossmeisl, J. Bridging the Catalyst Reactivity Gap between Au and Cu for the Reverse Water–Gas Shift Reaction. *J. Phys. Chem. C* **2022**, *126*, 19756–19765.

(51) Honkala, K.; Hellman, A.; Remediakis, I. N.; Logadottir, A.; Carlsson, A.; Dahl, S.; Christensen, C. H.; Nørskov, J. K. Ammonia Synthesis from First-Principles Calculations. *Science* **2005**, *307*, 555–558.

(52) Zhu, W.; Zhang, Y.-J.; Zhang, H.; Lv, H.; Li, Q.; Michalsky, R.; Peterson, A. A.; Sun, S. Active and Selective Conversion of CO_2 to CO on Ultrathin Au Nanowires. *J. Am. Chem. Soc.* **2014**, *136*, 16132–16135.

(53) Hvolbæk, B.; Janssens, T. V. W.; Clausen, B. S.; Falsig, H.; Christensen, C. H.; Nørskov, J. K. Catalytic Activity of Au Nanoparticles. *Nano Today* **2007**, *2*, 14–18.

(54) Haruta, M.; Daté, M. Advances in the Catalysis of Au Nanoparticles. *Appl. Catal. A: Gen.* **2001**, *222*, 427–437.

(55) Pedersen, J. K.; Clausen, C. M.; Skjegstad, L. E. J.; Rossmeisl, J. A Mean-Field Model for Oxygen Reduction Electrocatalytic Activity on High-Entropy Alloys**. *ChemCatChem* **2022**, *14*, e202200699.

(56) Yan, D.; Kristoffersen, H. H.; Pedersen, J. K.; Rossmeisl, J. Rationally Tailoring Catalysts for the CO Oxidation Reaction by Using DFT Calculations. *ACS Catal.* **2022**, *12*, 116–125.

(57) Gong, X.-Q.; Liu, Z.-P.; Raval, R.; Hu, P. A Systematic Study of CO Oxidation on Metals and Metal Oxides: Density Functional Theory Calculations. *J. Am. Chem. Soc.* **2004**, *126*, 8–9.

(58) Baxter, R. J.; Hu, P. Insight into Why the Langmuir–Hinshelwood Mechanism Is Generally Preferred. *J. Chem. Phys.* **2002**, *116*, 4379–4381.

(59) Wang, Z.; Hu, P. Rational Catalyst Design for CO Oxidation: A Gradient-Based Optimization Strategy. *Catal. Sci. Technol.* **2021**, *11*, 2604–2615.

(60) Christensen, O.; Hutu, A.-I.; Kristoffersen, H. H.; Rossmeisl, J. N_2 dissociation on AuCoFeMoRu high-entropy alloys: Circumventing scaling relations and step dependencies. *J. Catal.* **2024**, https://doi.org/10.1016/j.jcat.2024.115572.

(61) Lopez, N.; Janssens, T. V. W.; Clausen, B. S.; Xu, Y.; Mavrikakis, M.; Bligaard, T.; Nørskov, J. K. On the Origin of the Catalytic Activity of Gold Nanoparticles for Low-Temperature CO Oxidation. *J. Catal.* **2004**, *223*, 232–235.

(62) Remediakis, I. N.; Lopez, N.; Nørskov, J. K. CO Oxidation on Rutile-Supported Au Nanoparticles. *Angew. Chem. Int. Ed.* **2005**, *44*, 1824–1826.

(63) Loffler, T.; Ludwig, A.; Rossmeisl, J.; Schuhmann, W. What Makes High-Entropy Alloys Exceptional Electrocatalysts? *Angew. Chem., Int. Ed.* **2021**, *60*, 26894−26903.

(64) Clausen, C. M.; Pedersen, J. K.; Batchelor, T. A.; Rossmeisl, J. Lattice Distortion Releasing Local Surface Strain on High-Entropy Alloys. *Nano Res.* **2022**, *15*, 4775−4779.